buildings

MDPI

Article

Factors Controlling Heave Deformation of a High-Speed Railway Subgrade–Culvert Transition Section on an Expansive Soil Foundation: A Case Study of the Xi'an–Ankang High-Speed Railway

Qihuan Li [1], Tao Wu [2], Yangpeng Zhang [2], Hongri Zhang [2], Yuliang Lin [1], Zhen Zhang [3], Shiyi Luo [2], Zhihong Deng [1] and Jiming Yang [2,*]

[1] School of Civil Engineering, Central South University, Changsha 410075, China
[2] Guangxi Transportation Science and Technology Group Co., Ltd., Nanning 530029, China
[3] Railway Engineering Research Institute, China Academy of Railway Sciences Co., Ltd., Beijing 100081, China
* Correspondence: yangjim941031@126.com

Abstract

To reveal the heave deformation characteristics and influencing factors of high-speed railway subgrade–culvert transition section (SCTS) on expansive soil foundations under water immersion, this study takes the Xi'an–Ankang High-Speed Railway as the engineering background. An in situ vertical swelling pressure test was conducted, and the equivalent thermal expansion coefficient was back-calculated based on the temperature–moisture equivalence theory. A three-dimensional numerical model was then established. The effects of immersion zone width, swelling potential, and immersion location were analyzed. The results show that, as the immersion center gradually deviates from the culvert center, the maximum subgrade heave deformation exhibits a non-monotonic trend of first decreasing and then increasing. When the immersion zone is locally distributed beneath the culvert, differential heave deformation of the SCTS is likely to occur. Gray relational analysis indicates that the maximum heave deformation is highly associated with both immersion zone width and swelling potential, while the width of heave area is more closely associated with immersion zone width. In engineering practice, the immersion range of the foundation near the SCTS should be carefully controlled, and drainage, anti-seepage, waterproofing, and soil improvement measures should be adopted to reduce the risk of differential heave deformation.

Keywords: expansive soil foundation; transition section; heave deformation; swelling potential

Check for updates

Academic Editor: Cedric Payan

Received: 20 May 2026
Revised: 9 July 2026
Accepted: 21 July 2026
Published: 23 July 2026

Copyright: © 2026 by the authors. Licensee MDPI, Basel, Switzerland. This article is an open access article distributed under the terms and conditions of the Creative Commons Attribution (CC BY) license.

1. Introduction

Expansive soils are typical problematic engineering soils that exhibit significant swelling and shrinkage characteristics in environments with varying moisture [1,2]. With the continuous development of high-speed railway (HSR) construction in China, an increasing number of railway lines inevitably pass through expansive soil [3]. Although engineering measures such as excavation and replacement [4], physical improvement [5], or chemical stabilization [6] are frequently employed to treat expansive soil foundations, deep-seated expansive soils or soft rocks may still undergo continuous deformation due to water migration during the service period, constrained by engineering investment, construction

conditions, and treatment depth [7–10]. Engineering cases have shown that even expansive soil foundations or weakly expansive mudstone can swell after immersion [11–13], leading to railway subgrade heave and changes in track geometry.

To investigate the subgrade heave deformation characteristics of expansive soil foundations under water immersion conditions, existing studies have mostly relied on in situ tests to explore deformation evolution laws. For instance, scholars [14–18] conducted full-scale in situ water immersion tests to systematically grasp the swelling characteristics and subgrade heave laws of expansive soil foundations. Furthermore, Duan et al. [19–21] carried out scaled model tests on expansive soil foundations, revealing the transverse non-uniformity of subgrade heave induced by foundation swelling and its bottom-up transfer and attenuation mechanisms. These works have provided valuable data to support the understanding of expansive deformation laws. However, limited by high costs, physical tests struggle to simulate multiple conditions, necessitating further analysis combined with numerical simulations.

In terms of numerical simulation, Wang et al. [22,23] established a coupled FLAC3D-PFC3D model to analyze the effect of foundation swelling on subgrade heave deformation. However, the coupled finite element-discrete element method faces limitations in macro-scale engineering applications, such as difficulties in mesoscopic parameter calibration and high computational costs [24]. In contrast, the finite element analysis method based on the temperature–humidity equivalence principle [25,26] offers the advantages of computational convenience and clear engineering objectives. Based on this method, Duan et al. [27] investigated the influence of foundation water immersion on the mechanical and deformation characteristics of ballastless track subgrades. The equivalent thermal expansion coefficient is often calibrated using laboratory swelling pressure tests; incorporating in situ test results can provide better engineering representativeness.

The subgrade–culvert transition section (SCTS) is prone to differential deformation during its service period due to significant stiffness discontinuities. Existing studies have investigated the effects of construction methods [28] and structural degradation mechanisms [29] on the structural deformation of the SCTS, as well as the mitigating effects of auxiliary rails [30] and transition fills [31] on dynamic impact. Overall, current research primarily focuses on stiffness smoothing and dynamic response control under train loads [32]. However, studies on the heave deformation characteristics and primary controlling mechanisms of the SCTS structure under the direct water immersion of expansive soil foundations remain scarce.

In summary, existing studies have revealed the heave deformation characteristics of expansive soil foundations under water immersion through in situ immersion tests, model tests, and numerical simulations. These studies provide an important basis for understanding the heave deformation of expansive soil foundations and its influence on railway subgrade structures. However, most previous studies have focused on the deformation response of expansive soil foundation under global or localized water immersion, while less attention has been paid to the heave deformation characteristics of the stiffness-discontinuous SCTS under adverse water immersion conditions. In addition, the calibration of the equivalent thermal expansion coefficient in existing numerical simulations is mostly based on laboratory tests or empirical values, and field-based evidence from engineering cases remains limited. The influence mechanisms of immersion zone width, swelling potential, and immersion location on the heave deformation characteristics of subgrade–culvert transition sections still require further investigation.

To address these issues, this study takes the subgrade–culvert transition section on the expansive soil foundation of the Xi'an–Ankang High-Speed Railway as the engineering background. An in situ vertical swelling pressure test was conducted to obtain the

engineering-scale swelling pressure response of the expansive soil foundation under field constraint conditions after water immersion. The measured response provided a data basis for calibrating the equivalent thermal expansion coefficient in the temperature–moisture equivalence method. On this basis, the equivalent thermal expansion coefficient was back-calculated, and a three-dimensional finite element model of the high-speed railway SCTS on an expansive soil foundation was established. The effects of the equivalent thermal expansion coefficient, immersion zone width, and immersion location on subgrade heave deformation were systematically analyzed. The results are expected to provide a reference for drainage, anti-seepage design, and foundation heave control of high-speed railway SCTS in expansive soil regions.

2. Engineering Background and Design of the In Situ Test

2.1. Engineering Background

As shown in Figure 1, this study is based on the Xi'an–Ankang High-Speed Railway (HSR), which has a design speed of 350 km/h. The test site is located in the Ankang Basin, where expansive soils are widely distributed. The region has an average annual rainfall of 878 mm. Alternating high temperature and heavy rainfall induce intense wetting–drying cycles, resulting in frequent expansive-soil-related engineering problems. During construction, obvious surface cracks (Figure 1c) and several shallow slope failures (Figure 1d) were observed. According to the geotechnical investigation report, thick expansive soil deposits are widely distributed along the railway alignment, as shown in Figure 1e. The measured free swelling ratio ranges from 19% to 58%, the montmorillonite content ranges from 11.6% to 23.5%, and the cation exchange capacity ranges from 172 to 273 mmol/kg. According to the classification criteria in the Chinese railway design code TB 10025-2019 [33], the investigated soil can be classified as weakly to moderately expansive soil.

Affected by the swelling–shrinkage characteristics of the expansive soil, local water infiltration can readily induce pronounced differential heave deformation in the SCTS because of its discontinuous stiffness, thereby seriously threatening the track smoothness and operational safety of the HSR. To investigate the swelling response of the expansive soil foundation under localized fully immersed conditions and to provide reliable physical calibration parameters for subsequent structural deformation analysis, an in situ vertical swelling pressure test was designed and conducted in this study.

2.2. Design of the In Situ Vertical Swelling Pressure Test of Expansive Soil Foundation

The vertical swelling pressure induced by water immersion in the expansive soil foundation of the test area provides an important parameter for the numerical simulation of water-immersion-induced foundation heave. Compared with free swelling ratio tests or laboratory swelling pressure tests, the in situ test better represents the actual boundary conditions of the foundation and can simultaneously reflect the effects of the water content of undisturbed soil and the immersion process on heave deformation characteristics.

As shown in Figure 2a, the in situ vertical swelling pressure test site had a planar dimension of approximately 6 m × 5 m and was formed by excavating the expansive soil foundation to a depth of 0.3 m. The water immersion zone was located at the center of the site, where a 0.707 m × 0.707 m steel plate was placed as the loading plate, and the designed immersion depth was 3 m. Controlled loading was achieved using a reaction system assembled with a hydraulic jack. As shown in Figure 2b, undisturbed expansive soil samples at different depths were collected by drilling before and after the test, and their water contents were determined using the oven-drying method. The specific testing procedures were as follows:

1. Site leveling and immersion pipe installation. As shown in Figure 2c, five 3 m-deep holes, as illustrated in Figure 2b, were drilled in the excavated and leveled site. Interconnected water pipes were then inserted, and the gaps between the pipes and the boreholes were filled with gravel. The water pipes were perforated in advance to allow water discharge from the pipes and infiltration into the surrounding soil.
2. As shown in Figure 2d, four earth pressure cells were installed, followed by backfilling with fine sand.
3. According to Figure 2a,e, the loading plate was first placed over the test area, followed by the installation of the hydraulic jack and the arrangement of the main and secondary steel beams. Concrete blocks were then stacked to provide the counterweight reaction force.
4. As shown in Figure 2f, four dial gauges were installed at the four corners of the loading plate. At this stage, the test setup was completed.
5. During the test, water was continuously supplied to the immersion system through a water tank. Meanwhile, the readings of the earth pressure cells were recorded, and the stroke of the hydraulic jack was adjusted in time according to the dial gauge readings, ensuring that the vertical swelling pressure of the foundation and the reaction force of the jack remained coordinated.

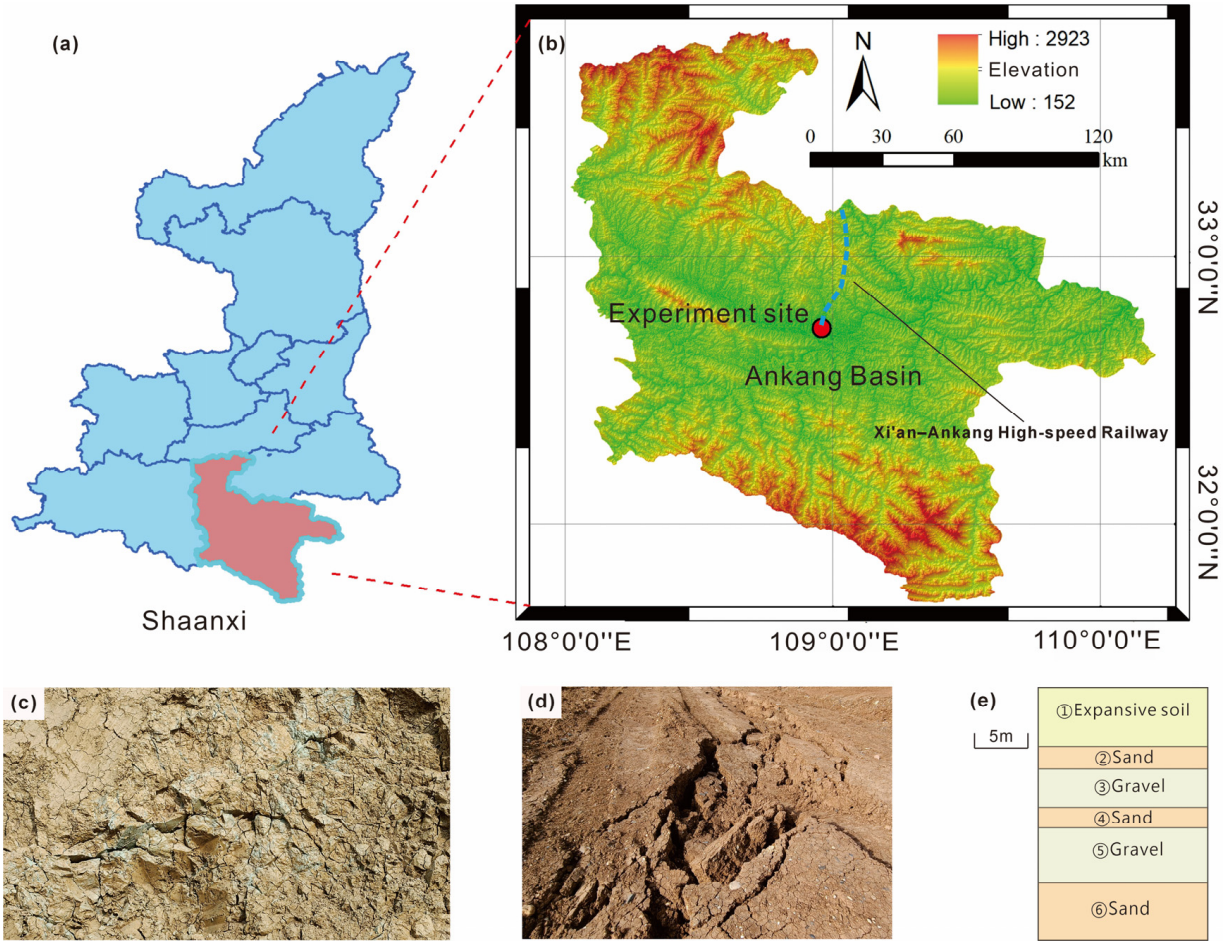

Figure 1. Engineering background of the test site: (**a**) geographical location of the test area; (**b**) topographic map of the Ankang Basin and the test site; (**c**) fissured expansive soil; (**d**) shallow landslide in expansive soil observed during construction; (**e**) soil layer distribution at the test site.

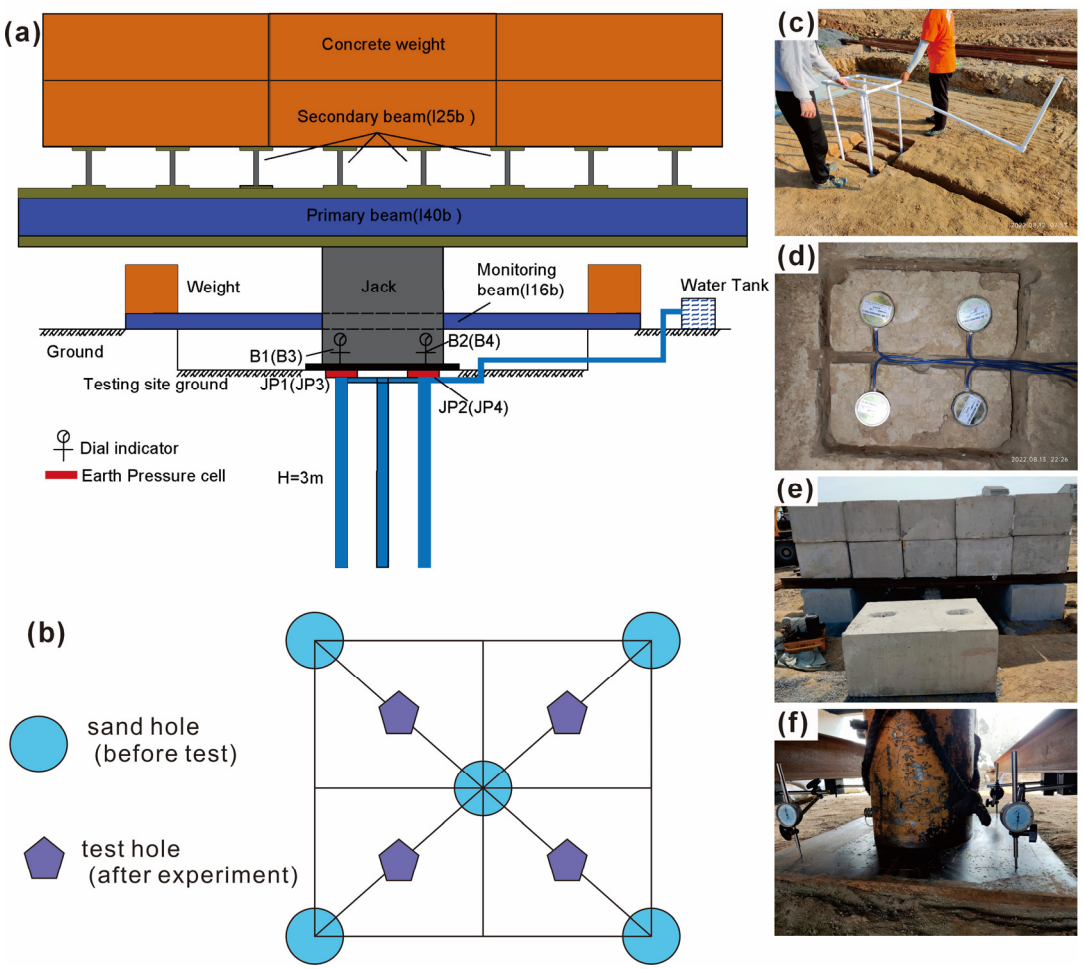

Figure 2. In situ vertical swelling pressure test: (**a**) test design; (**b**) water content test before and after the test; (**c**) installation of the water immersion pipe; (**d**) layout of earth pressure cells; (**e**) installation of the reaction frame; (**f**) installation of the hydraulic jack.

2.3. Results of the In Situ Vertical Swelling Pressure Test

The variation in the water content of the foundation soil with depth, measured from borehole samples before and after the test, is shown in Figure 3a. Before water immersion, the natural water content of the site soil mainly ranged from 15% to 20%. After continuous water injection, the water content of the shallow soil layer at depths of 0–1.5 m increased significantly, reaching a maximum of approximately 25–27%. This indicates that the designed sand-filled water-injection holes effectively promoted the downward infiltration of water. However, below a depth of 1.5 m, the increase in water content gradually decreased, and the curve nearly coincided with the initial water content curve below 2.0 m. This depth-dependent decrease in water content increment after the immersion test reflects the low permeability of overconsolidated expansive soil and further indicates that moisture diffusion had reached a dynamic equilibrium in the later stage of the test.

The results of the in situ vertical swelling pressure test are shown in Figure 3b. The monitoring results of SP1–SP4 indicate that the readings of all earth pressure cells generally exhibited an “S-shaped” increasing trend with immersion time, which can be divided into three stages: initial response, rapid growth, and final stabilization. At the early stage of immersion, the water content of the soil gradually increased, and the swelling pressure increased slowly. As water further infiltrated into the soil, the water-absorption swelling of the expansive soil intensified, leading to a rapid increase in earth pressure. When the

water-content state and boundary constraints of the soil gradually became stable, the earth pressure readings entered the stabilization stage.

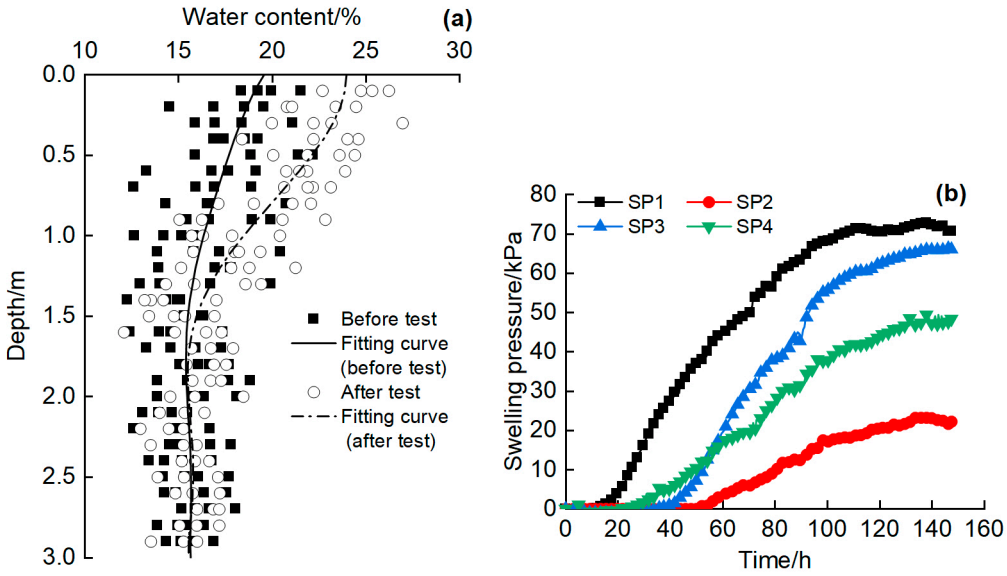

Figure 3. Results of the in situ test: (**a**) variation in water content before and after the test; (**b**) variation in vertical swelling pressure.

The in situ vertical swelling pressure test was affected by the heterogeneity of the field strata and the loading boundary conditions; therefore, the readings of the earth pressure cells at different locations showed certain differences. The possible reasons are as follows: (1) the water content, pore structure, crack development, and distribution of expansive clay minerals in the test area were spatially heterogeneous, resulting in asynchronous water-absorption swelling processes and swelling pressure development at different locations after immersion; (2) the lateral constraint conditions of the soil around the loading plate varied. When the lateral constraint was relatively strong, the lateral deformation of the soil beneath the loading plate was restricted, resulting in a relatively large vertical swelling pressure. In contrast, when the lateral constraint was relatively weak, the soil was able to deform laterally more sufficiently, resulting in a relatively small vertical swelling pressure; and (3) it was difficult to ensure complete coincidence between the center of the jack and the center of the loading plate. Eccentric loading may have caused a slight inclination of the loading plate, leading to differences in the stress states of the earth pressure cells at different locations.

Under the combined influence of the above factors, the final stable reading of SP2 was significantly lower than those of SP1, SP3, and SP4, and deviated from the stable reading group formed by the other three earth pressure cells. Considering that the subsequent calibration of the equivalent thermal expansion coefficient requires a representative vertical swelling pressure of the expansive soil foundation beneath the loading plate, SP2 was treated as a local anomalous reading and was not included in the calculation of the representative value. Finally, the average value of the stable-stage readings of SP1, SP3, and SP4 was taken as the in situ vertical swelling pressure. The vertical swelling pressure of the expansive soil foundation in the test area was determined to be approximately 61.5 kPa, which was used as the calibration value for the subsequent numerical analysis.

3. Numerical Simulation of Subgrade Heave Deformation in the Subgrade–Culvert Transition Section

3.1. Simulation Theory of Expansive Soil Swelling Characteristics Based on Thermo-Mechanical Coupling Analysis

The moisture-induced swelling of expansive soil is essentially governed by variations in water content and matric suction. In this study, all numerical simulations were performed using ABAQUS 2020. To simulate volumetric swelling induced by moisture variation in general-purpose finite element software, this study adopts a temperature–moisture equivalence approach. This approach is based on the mathematical similarity between the governing equation of unsaturated seepage and the heat conduction equation. Accordingly, the moisture field can be equivalently represented by a temperature field. In this way, the moisture-induced swelling strain can be simulated by thermal expansion strain. The transient seepage continuity equation for unsaturated soil based on Darcy's law is given in Equation (1), and Fourier's heat conduction equation is given in Equation (2):

$$\frac{\partial}{\partial x}\left(k_x\frac{\partial h_w}{\partial x}\right)+\frac{\partial}{\partial y}\left(k_y\frac{\partial h_w}{\partial y}\right)+\frac{\partial}{\partial z}\left(k_z\frac{\partial h_w}{\partial z}\right)=C_w\frac{\partial h_w}{\partial t} \tag{1}$$

$$\frac{\partial}{\partial x}\left(\lambda_x\frac{\partial T}{\partial x}\right)+\frac{\partial}{\partial y}\left(\lambda_y\frac{\partial T}{\partial y}\right)+\frac{\partial}{\partial z}\left(\lambda_z\frac{\partial T}{\partial z}\right)=\rho C_V\frac{\partial T}{\partial t} \tag{2}$$

where h_w is the matric suction head; k_i (i = x,y,z) is the permeability coefficient in each direction; C_w is the specific water capacity; t is time; T is temperature; λ_i (i = x,y,z) is the thermal conductivity in each direction; ρ is density; and C_V is the specific heat capacity.

A comparison between Equations (1) and (2) shows that the two equations have highly similar mathematical forms. Therefore, the equivalence between the moisture field and the temperature field can be established through parameter mapping. The swelling–shrinkage deformation of expansive soil induced by moisture variation can be expressed by Equation (3), while the deformation induced by temperature variation can be calculated using Equation (4):

$$\Delta\varepsilon_{ij}^{w}=\beta\delta_{ij}C_w\Delta h=\beta\delta_{ij}\Delta w \tag{3}$$

$$\Delta\varepsilon_{ij}^{T}=\alpha\delta_{ij}\Delta T \tag{4}$$

where $\Delta\varepsilon_{ij}^{w}$ is the swelling strain caused by the change in water content; β is the moisture-induced swelling coefficient; δ_{ij} is the Kronecker delta; Δh is the change in matric suction head; Δw is the change in water content; $\Delta\varepsilon_{ij}^{T}$ is the strain induced by temperature change; α is the thermal expansion coefficient; and ΔT is the temperature change.

In the numerical simulation, the thermal expansion strain is assumed to be equivalent to the moisture-induced swelling strain. By equating Equations (3) and (4), the following relationship can be obtained:

$$\alpha=\frac{\beta\Delta w}{\Delta T} \tag{5}$$

In this study, the expansive soil was assumed to have the same swelling potential in the three principal directions. The equivalent thermal expansion coefficient α obtained from Equation (5) was then introduced into the thermo-mechanical coupling module of ABAQUS. By prescribing a temperature change, the moisture-induced swelling deformation of expansive soil was equivalently represented by thermal expansion strain, so as to simulate the heave deformation of expansive soil foundations induced by wetting [34].

3.2. Calculation of Equivalent Thermal Expansion Coefficient

To back-calculate the equivalent thermal expansion coefficient, a three-dimensional calibration model corresponding to the in situ vertical swelling pressure test was first established. As shown in Figure 4a, the model dimensions were 16 m × 15 m × 5 m. A 0.3 m excavation was introduced in the central area to reproduce the field test condition. The immersion-swelling zone was located at the center of the model, with a planar size of 0.707 m × 0.707 m and an immersion depth of 3 m. Concrete support areas for the reaction system were arranged on both sides of the central test area.

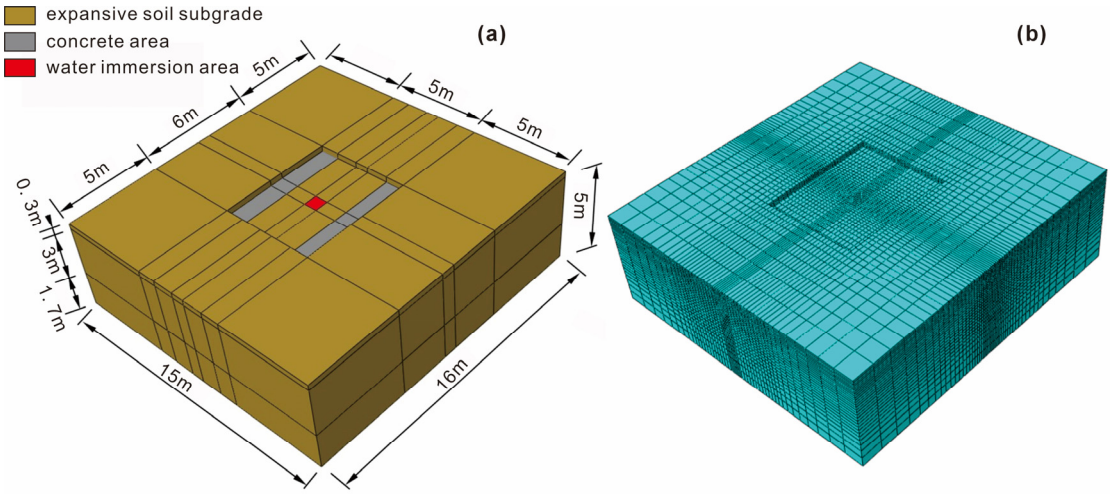

Figure 4. Calibration procedure for the equivalent thermal expansion coefficient: (**a**) schematic model; (**b**) mesh of the model.

The finite element modeling and calculation were conducted using the general-purpose finite element software ABAQUS (version 2020). The mesh configuration of the model is shown in Figure 4b. The expansive soil was described using the Mohr–Coulomb model, and its parameters were determined based on laboratory tests conducted according to the relevant Chinese national standards. The elastic modulus, Poisson's ratio, density, cohesion, and internal friction angle of the expansive soil foundation were set as 12 MPa, 0.30, 1900 kg/m^3, 27 kPa, and 15°, respectively.

Normal displacement constraints were applied to the lateral and bottom boundaries of the model. A load of approximately 6 kPa, corresponding to the self-weight of the loading plate and jack, was applied to the surface of the immersion-swelling zone. A load of approximately 67.5 kPa, corresponding to the self-weight of the reaction system, was applied to the concrete support areas. After the geostatic stress equilibrium was established, the water-content fields before and after immersion were equivalently converted into the initial temperature field and the elevated temperature field, respectively. A uniformly distributed constraining load of 61.5 kPa was then applied to the surface of the immersion zone.

The equivalent thermal expansion coefficient was determined through an iterative calibration procedure. Specifically, the thermal expansion coefficient was gradually adjusted until the vertical displacement of the immersion-swelling zone approached zero under the applied constraining load. The corresponding thermal expansion coefficient was then taken as the equivalent thermal expansion coefficient. The calibrated reference equivalent thermal expansion coefficient was determined to be 7.228 × 10^{-4} °C^{-1}.

3.3. Three-Dimensional Finite Element Model of the Subgrade–Culvert Transition Section on an Expansive Soil Foundation

The numerical model was established based on the typical double-track railway subgrade structure specified in the design code in China [35]. The subgrade was 3.0 m high and 13.8 m wide at the surface, with a side slope gradient of 1:1.5 and a center-to-center track spacing of 5.0 m. The surface layer of the subgrade bed was 0.7 m thick, and the bottom layer was 2.3 m thick. To minimize the influence of lateral boundary constraints on the calculation results, the total length and width of the model were set to 100 m and 42.8 m, respectively. The culvert was located at the middle of the model, with its centerline 50 m from either longitudinal end of the model, and was arranged orthogonally to the subgrade. The culvert was 2.3 m high and 3.0 m wide, with a uniform thickness of 0.2 m for the roof slab, floor slab, and sidewalls. The SCTS was arranged in an inverted trapezoidal form, with a bottom width of 2.0 m, and the connection slope between the SCTS and the ordinary subgrade was 1:2. Based on the geological survey data, the foundation was modeled as a 10 m-deep expansive soil layer. The established numerical model is shown in Figure 5.

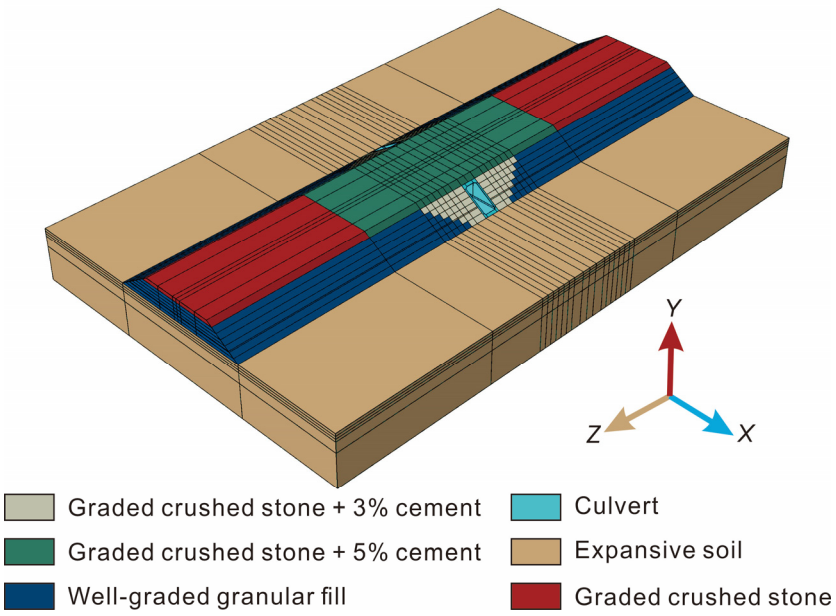

Figure 5. Three-dimensional finite element model of a high-speed railway subgrade–culvert transition section on an expansive soil foundation.

The model was discretized using C3D8 elements. To improve computational accuracy while maintaining computational efficiency, the mesh was refined near the culvert and appropriately coarsened in areas far from the culvert. The mesh distribution was optimized through several trial calculations, and the final model contained 32,330 elements and 39,624 nodes. Surface-to-surface contact was adopted between the culvert and the surrounding fill. The normal behavior was defined as hard contact, and the tangential behavior was simulated using the penalty formulation with a friction coefficient of 0.3. Normal displacement constraints were applied to the bottom and lateral boundaries of the model.

In terms of material assignment, the bottom layer of the subgrade bed was filled with Group A fill material, while the transition section was filled with graded crushed stone mixed with 3% cement. The surface layer above the bottom layer was filled with graded crushed stone, whereas the surface layer above the transition section was filled with graded crushed stone mixed with 5% cement. The culvert was constructed with C35 concrete. Because this study focuses on the heave deformation characteristics of an expansive soil

foundation after water immersion, the time-dependent constitutive evolution governed by water-content variation during the wetting process was not considered. Therefore, the subgrade fill and expansive soil foundation were both defined using the Mohr–Coulomb model. The constitutive models proposed by Zhao et al. [36–38] may provide useful references for future investigations of the deformation and stress state of railway subgrades under long-term service conditions. The culvert was simulated using a linear elastic model.

The parameters of the fill materials listed in Table 1 were determined by comprehensively referring to the studies of Deng [39] and Cai [40], whereas the parameters of the expansive soil were obtained from laboratory tests conducted according to the Code for Soil Test of Railway Engineering (TB 10102-2010) in China [41].

Table 1. Main material parameters of the numerical model.

Material	*E*/MPa	*ν*	*ρ*/(kg·m^{-3})	*c*/kPa	*φ*/(°)
Graded crushed stone	150	0.30	2200	75	25
Graded crushed stone and 3% cement	180	0.30	2200	75	27
Graded crushed stone and 5% cement	580	0.24	2200	75	35
Well-graded granular fill	100	0.30	2000	55	20
Expansive soil	12	0.30	1900	27	15
C35 concrete	31,500	0.20	2500	-	-

Uniformly distributed loads were applied to the subgrade surface to represent the self-weight of the track structure and the fill between the two tracks. The load induced by the self-weight of the track structure was 17.3 kN/m^2, with a distribution width of 3.4 m, while the load induced by the fill between the two tracks was 10.7 kN/m^2, with a distribution width of 1.6 m.

3.4. Setup of Water Immersion Conditions and Simulation Cases

As shown in Figure 6, the water immersion conditions of the expansive soil foundation were divided into two types: complete immersion and localized immersion. Because localized immersion is more representative of actual engineering conditions, this study focused on the effects of three variables under localized immersion, namely the immersion zone width, swelling potential, and immersion zone location. The simulation cases are listed in Table 2. Different immersion conditions were simulated by changing the immersion zone width (L), thermal expansion coefficient (α), and central position of the immersion zone in the numerical model.

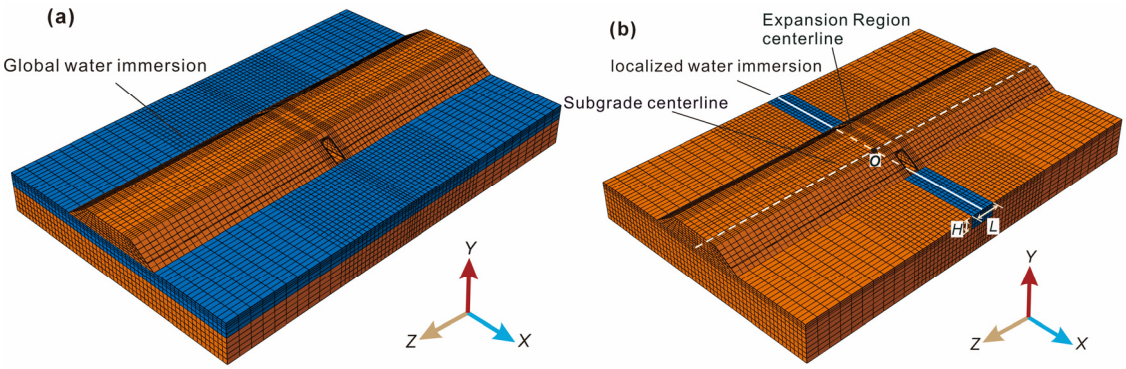

Figure 6. Setup of water immersion conditions: (**a**) global water immersion; (**b**) local water immersion.

Table 2. Numerical modeling cases.

Analysis Factor	Variable Value	Fixed Condition
Width of the water immersion zone (L)/m	2, 4, 6, 8, 10	X_d = 0 m, α = 7.228 × 10^{-4} °C^{-1}
Swelling potential (α)/(1 × 10^{-4} °C^{-1})	5, 6, 7.228, 8, 9	L = 6 m, X_d = 0 m
Location of the water immersion zone (X_d)/m	0, 3, 6, 9, 12, 18, 24, 30	L = 6 m, α = 7.228 × 10^{-4} °C^{-1}

According to the expansive soil region design standard in China [42], the depth of atmospheric influence for the expansive soil at the test site is 3.5 m; therefore, the groundwater table depth was assumed to be 3.5 m. Because the water content of the soil below the groundwater table remains relatively stable, the main swelling zone in the model was set within the expansive soil layer at a depth of 0–3.5 m. The initial water content of the swelling zone before immersion was taken as 20.9%, and the water content after immersion was set to 26.4%. Correspondingly, in the equivalent temperature field, the initial temperature was set to 20.9 °C, and the target temperature after heating was set to 26.4 °C. By increasing the temperature of the swelling zone to induce thermal expansion, the swelling deformation caused by moisture variation was equivalently simulated. As shown in Figure 7, after heating, the main swelling zone reached 26.4 °C. Owing to heat conduction, a noticeable temperature rise was also observed within 0.8 m below the swelling zone.

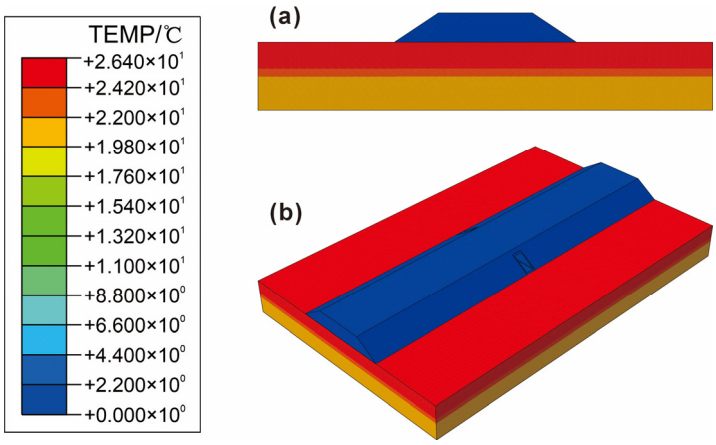

Figure 7. Temperature field in subgrade when warming to 26.4 °C was applied to swelling area: (**a**) cross view; (**b**) oblique view.

In this study, the maximum heave deformation (H) and width of heave area (W) were selected as the main response indicators. The maximum heave deformation H reflects the overall deformation amplitude of the subgrade surface, whereas the width of heave area W reflects the longitudinal influence length of the deformation along the railway line. In addition, the heave gradient and differential deformation near the culvert induced by localized water immersion were also examined.

4. Results and Discussion

4.1. Subgrade Heave Characteristics Under Global and Local Water Immersion Conditions

It can be seen from Figure 8, compared with localized immersion-induced swelling of the foundation, large-area immersion-induced swelling causes an overall uplift of the railway subgrade. Under this condition, although the magnitude of surface heave is larger, the non-uniformity of the heave deformation along the longitudinal direction of the subgrade is reduced. Considering the high operating speed of HSR trains, even small non-uniform heave deformation may significantly affect train operation and threaten the

safety of train operation and passengers. In addition, railway subgrades are often subjected to various unfavorable conditions during long-term service. Therefore, to account for relatively unfavorable conditions, localized immersion-induced swelling of the foundation was assumed in all subsequent simulations. The effects of the location, size, and swelling potential of the localized immersion zone on the deformation characteristics of the railway subgrade were then analyzed.

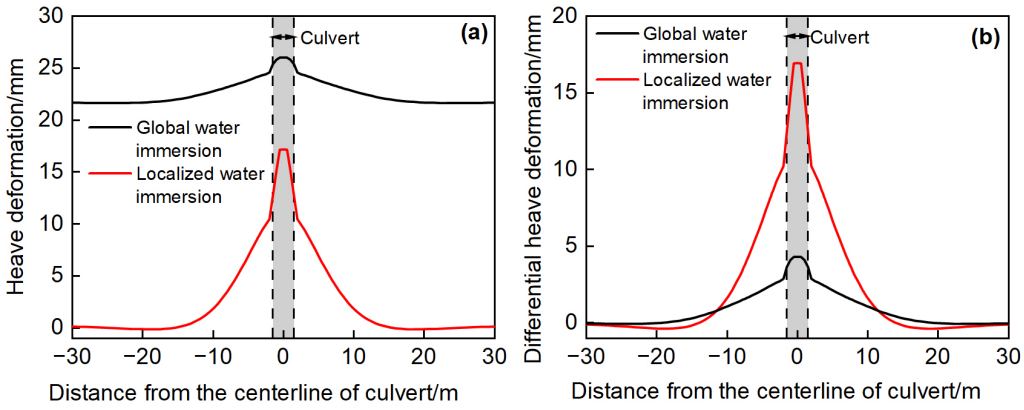

Figure 8. Heave deformation of the railway subgrade under global and local water immersion conditions: (**a**) subgrade heave deformation; (**b**) differential subgrade heave deformation.

4.2. Evolution of Subgrade Heave Deformation Under Varying Water Immersion Widths

Figures 9 and 10 show the influence of the immersion zone width of the expansive soil foundation on the heave deformation characteristics of the subgrade. As the immersion zone width increased from 2 m to 10 m, the maximum heave of the subgrade surface increased from 8.746 mm to 22.495 mm, corresponding to an increase of approximately 157.2%. Meanwhile, the width of heave area increased from 22.648 m to 32.656 m, corresponding to an increase of approximately 44.2%. This indicates that the immersion zone width not only directly controls the volume of expansive soil involved in deformation, but also expands the transfer range of heave deformation along the railway alignment. From the perspective of incremental variation, when L increased from 2 m to 6 m, the maximum heave deformation increased by 8.192 mm and the width of heave area increased by 5.604 m. When L increased from 6 m to 10 m, the maximum heave increased by only 5.557 mm and the width of heave area increased by 4.404 m. This suggests that the influence of increasing immersion width on the heave response gradually weakens.

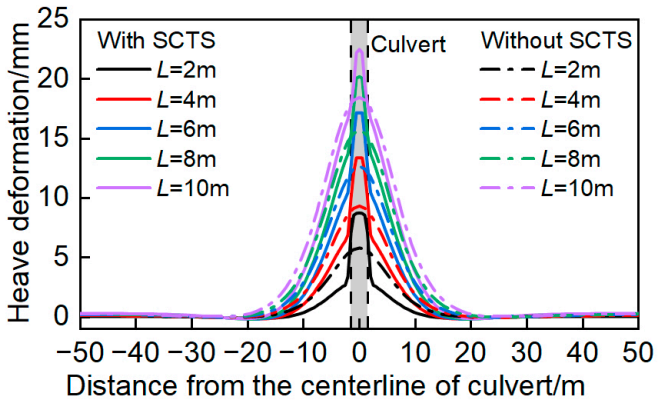

Figure 9. Effect of water immersion zone width on the heave deformation of the railway subgrade.

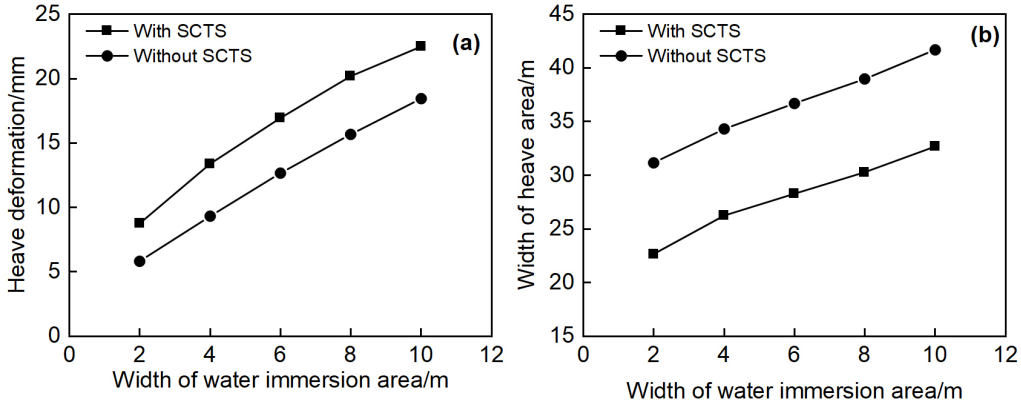

Figure 10. Effect of water immersion zone width on heave characteristics: (**a**) subgrade heave deformation; (**b**) width of heave area.

Taking the case with an immersion zone width of L = 6 m as an example, as shown in Figure 11, compared with the subgrade without a culvert, the subgrade with a culvert exhibited a larger maximum surface heave but a smaller width of heave area, which would aggravate track irregularity. For the subgrade with a culvert, the relatively small self-weight load of the culvert resulted in a significant increase in surface heave at the culvert location. In contrast, the transition section fills on both sides of the culvert had a larger unit weight, which reduced the width of heave area on the subgrade surface.

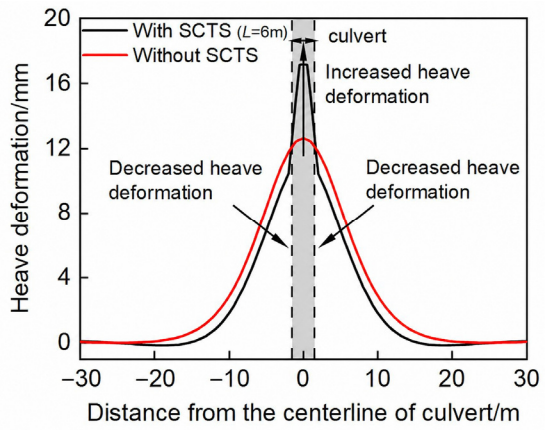

Figure 11. Comparison of subgrade heave deformation with and without a subgrade–culvert transition section.

Figure 12 shows the variation rate of subgrade surface heave deformation, namely the heave gradient. When the SCTS was arranged in the subgrade, the heave gradient of the subgrade surface changed abruptly at the culvert location. Specifically, when no culvert was arranged in the subgrade, the maximum heave gradient of the subgrade surface was 1.309 mm/m. When an SCTS was arranged in the subgrade, the maximum heave gradient increased to 4.886 mm/m. Therefore, to ensure track regularity, drainage and waterproofing measures should be strengthened for the foundation near the culvert. In addition, reasonable SCTS fills should be selected, the layout of the SCTS should be optimized, and reinforcement measures such as geogrids or steel meshes should be adopted to reduce the heave gradient of the subgrade surface near the culvert, thereby ensuring smooth train operation at the design speed. From an engineering perspective, it is recommended to minimize the width of the immersion zone in expansive soil foundations and control it within 4 m where possible.

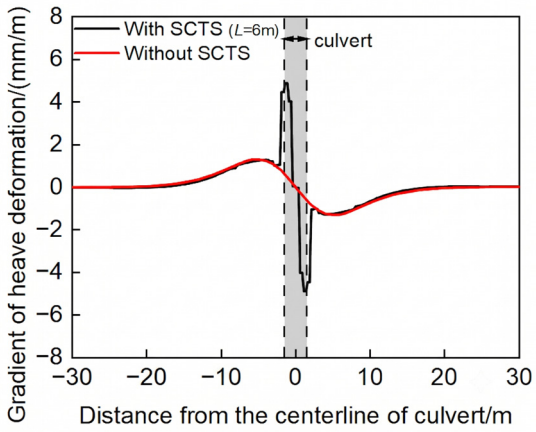

Figure 12. Comparison of subgrade heave deformation gradients with and without a subgrade–culvert transition section.

4.3. Effect of Swelling Potential on Subgrade Heave Deformation

Keeping the location and size of the foundation immersion-swelling zone unchanged, the variation in the swelling potential of the immersion zone was simulated by changing the equivalent thermal expansion coefficient (α), so as to analyze its influence on the railway subgrade. The heave deformation at the track centerline on the subgrade surface under different swelling potentials is shown in Figure 13. The relationships between the maximum surface heave, the width of the heave area, and the swelling potential of the foundation immersion zone are shown in Figure 14. It can be seen that, under the same swelling potential, compared with the subgrade without a culvert, the subgrade with a culvert exhibited a larger maximum surface heave but a smaller width of the heave area, which is consistent with the previous simulation results.

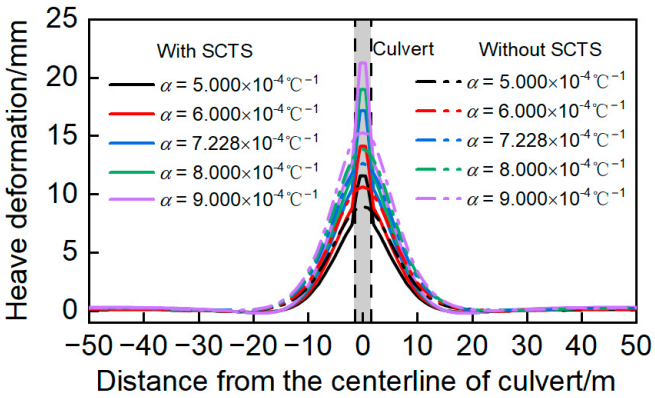

Figure 13. Effect of swelling potential on the subgrade heave deformation.

As the swelling potential of the foundation immersion zone increased, the maximum surface heave of the subgrade increased significantly, whereas the width of the heave area changed only slightly. Taking the subgrade with a culvert as an example, when the equivalent thermal expansion coefficient (α) of the foundation immersion zone was 5.0×10^{-4} °C^{-1}, the maximum surface heave of the subgrade was 11.585 mm, and the width of heave area was 27.5 m. When α increased to 9.0×10^{-4} °C^{-1}, the maximum surface heave increased to 21.288 mm, corresponding to an increase of approximately 83.8%, whereas the width of heave area increased only to 28.5 m, corresponding to an increase in merely 3.6%.

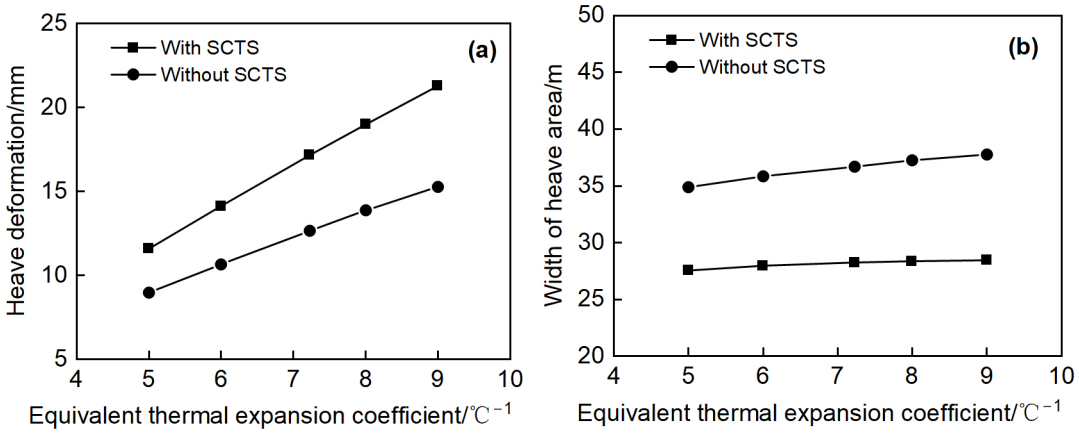

Figure 14. Effect of swelling potential on heave characteristics: (**a**) subgrade heave deformation; (**b**) width of heave area.

The heave gradients of the subgrade surface corresponding to different thermal expansion coefficients are shown in Figure 15. As the equivalent thermal expansion coefficient of the foundation immersion zone increased, the heave gradient of the subgrade surface increased significantly. Compared with the subgrade without a culvert, the subgrade with a culvert exhibited a greater variation in the surface heave gradient. Specifically, when the equivalent thermal expansion coefficient (α) of the foundation immersion zone increased from 5.0×10^{-4} °C^{-1} to 9.0×10^{-4} °C^{-1}, the heave gradient of the subgrade without a culvert increased from 0.927 mm/m to 1.615 mm/m, corresponding to an increase of approximately 74.2%. In contrast, the heave gradient of the subgrade with a culvert increased from 3.484 mm/m to 6.559 mm/m, corresponding to an increase of approximately 88.3%.

The results show that the increase in the swelling potential parameter α increases the heave deformation of the expansive soil foundation. In addition, the deformation gradient beneath the culvert becomes larger, which may have an adverse effect on the SCTS. Improving expansive soil can reduce the swelling potential of the foundation soil and thus mitigate engineering problems induced by swelling–shrinkage deformation. Chemical stabilization, such as the addition of cement and lime, has been reported to modify the properties of expansive soil and significantly reduce its swelling–shrinkage potential [8]. Physical improvement methods, such as the incorporation of fiber materials including bagasse fibers, can improve the engineering strength of expansive soil and limit swelling–shrinkage deformation [5]. Nevertheless, expansive soil improvement generally involves practical difficulties and relatively high costs. In engineering practice, soil replacement is therefore commonly adopted to reduce the swelling potential of expansive soil foundations [43].

4.4. Response of Water Immersion Zone Location to Subgrade Heave Deformation

The distance between the centerline of the foundation immersion zone and the centerline of the culvert is defined as X_d. By changing X_d in the numerical model, the influence of the immersion zone location on the heave deformation characteristics of the railway subgrade was investigated. As shown in Figure 16, with the increase in the distance between the centerline of the foundation immersion zone and the culvert centerline, the maximum heave at the track centerline on the subgrade surface showed a trend of first decreasing, then increasing, and finally tending to stabilize. When X_d increased from 0 m to 6 m, the maximum heave at the track centerline decreased from 17.213 mm to 10.464 mm. When X_d increased from 6 m to 24 m, the maximum heave increased from 10.464 mm to 12.584 mm. When X_d further increased from 24 m to 30 m, the maximum heave showed no obvious change.

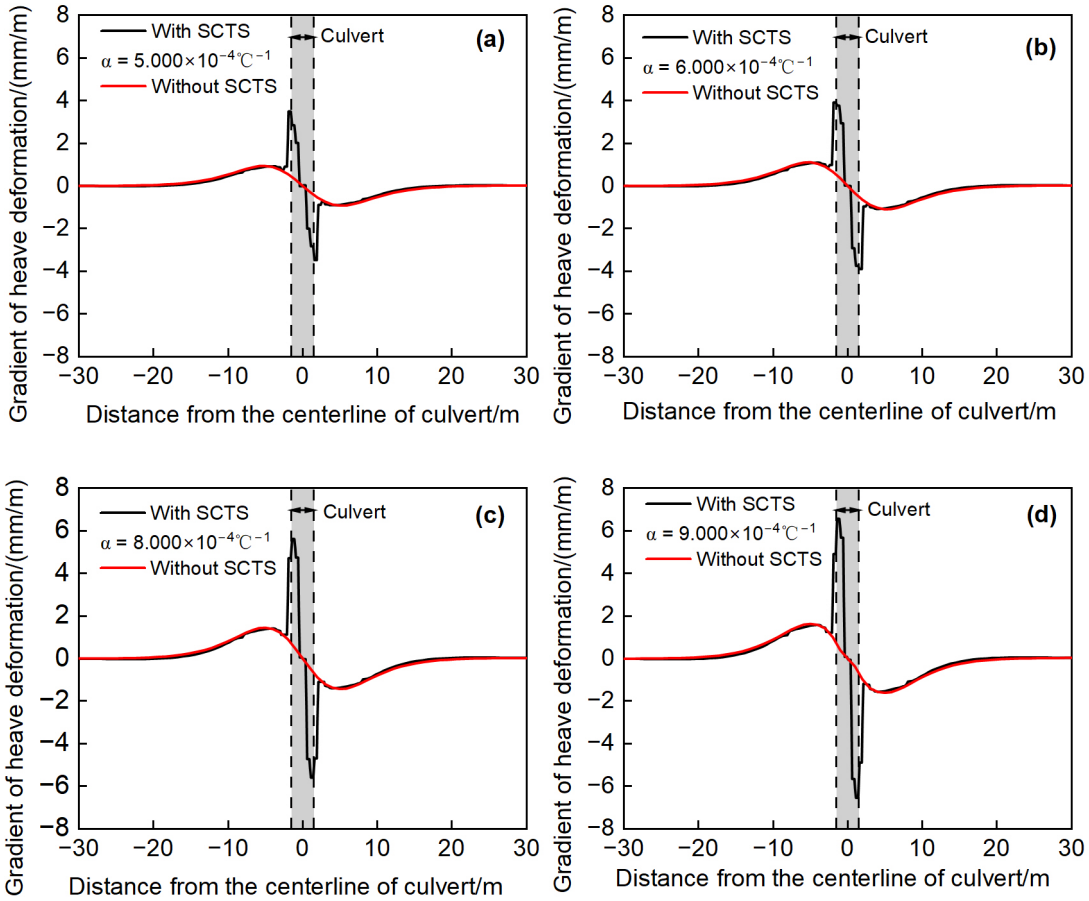

Figure 15. Heave deformation gradients of the railway subgrade under different swelling potentials of the infiltration zone: (**a**) $\alpha = 5.0 \times 10^{-4}\ ^{\circ}C^{-1}$; (**b**) $\alpha = 6.0 \times 10^{-4}\ ^{\circ}C^{-1}$; (**c**) $\alpha = 8.0 \times 10^{-4}\ ^{\circ}C^{-1}$; (**d**) $\alpha = 9.0 \times 10^{-4}\ ^{\circ}C^{-1}$.

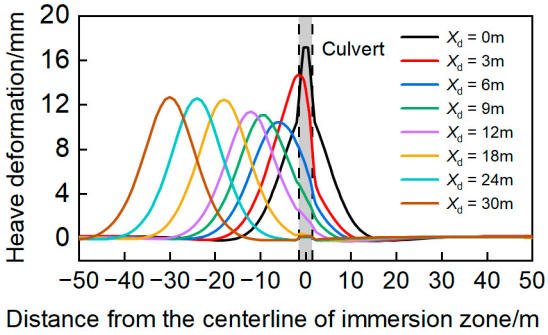

Figure 16. Effect of water immersion zone location on subgrade heave deformation.

This phenomenon can be attributed to the difference in overburden load above the foundation. The mass of the culvert is smaller than that of the subgrade soil with the same volume; therefore, compared with the foundation beneath the ordinary subgrade, the foundation beneath the culvert is subjected to a smaller overburden load. In contrast, because the SCTS fill has a larger unit weight, the foundation beneath the SCTS is subjected to a larger overburden load than that beneath the ordinary subgrade. Under the same conditions, a larger overburden load leads to smaller swelling deformation of the soil. Therefore, within a certain distance from the culvert, under the combined influence of the culvert and the SCTS, the maximum heave at the track centerline on the subgrade surface shows a decreasing-then-increasing trend as X_d increases. When the foundation immersion zone is far from the culvert, the influence of the SCTS on the overburden load of

the foundation becomes limited. Consequently, the maximum heave at the track centerline shows no obvious change with a further increase in X_d.

As shown in Figure 17, the width of heave area also exhibited a non-monotonic variation with the change in immersion location. When X_d was 18 m, the width of heave area reached 35.824 m, which was the maximum value among this group of cases. In contrast, when X_d was 0 m and X_d was 3 m, the width of heave area was approximately 28.2 m. These results indicate that the immersion location mainly controls the deformation distribution pattern and width of heave area, rather than only affecting the peak heave. For the SCTS, when the immersion zone is located directly beneath the culvert, it may cause the overall uplift of the culvert. When the immersion zone is located near the culvert but not directly beneath it, differential deformation on one side of the culvert may be induced, which may adversely affect smooth railway operation. From an engineering perspective, the distance between the center of the immersion zone and the centerline of the SCTS should be increased as much as possible. It is recommended to keep X_d greater than 9 m so that the foundation heave deformation after immersion can be controlled within 5 mm.

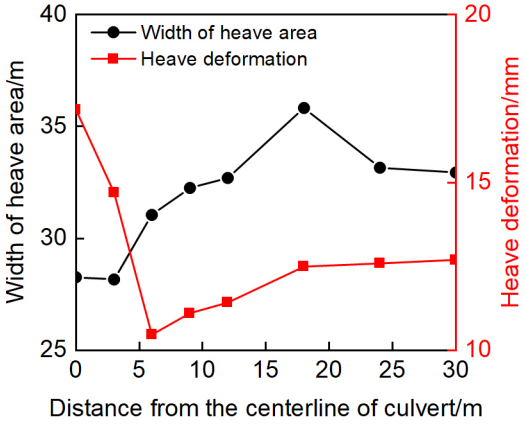

Figure 17. Effect of water immersion zone location on subgrade heave characteristics.

It should be noted that when no culvert is arranged in the railway subgrade, or when the foundation immersion zone is far from the culvert, the immersion zone location has no obvious influence on the heave deformation of the railway subgrade. Therefore, to more clearly illustrate the influence of the immersion zone location on subgrade heave deformation, the subgrade surface heave deformations corresponding to different immersion zone locations were compared with those under the no-culvert condition, as shown in Figure 18. The results show that the heave deformation of the railway subgrade surface tends to develop toward the side with weaker constraints. When X_d was 3 m or 6 m, the subgrade heave deformation developed toward the culvert side. When X_d was 12 m, the SCTS had a significant influence on the heave deformation, causing the subgrade heave deformation to develop away from the culvert side. When X_d was 24 m, the subgrade heave deformation was almost unaffected by the SCTS.

Based on the above analysis, when the foundation immersion zone is located directly beneath the culvert, the maximum heave deformation occurs on the subgrade surface. In this case, the culvert undergoes overall uplift. When the foundation immersion zone is not directly beneath the culvert but is close to it, the subgrade surface heave deformation tends to develop toward the culvert side, leading to a more non-uniform deformation pattern in the SCTS. Therefore, for railway subgrades constructed in expansive soil regions, drainage, waterproofing, and swelling-reduction measures should be strengthened near the culvert. Localized water immersion and swelling of the foundation beneath or near the culvert

should be avoided, so as to reduce large subgrade heave and its adverse influence on the culvert, thereby ensuring the normal service of the culvert within its design service life.

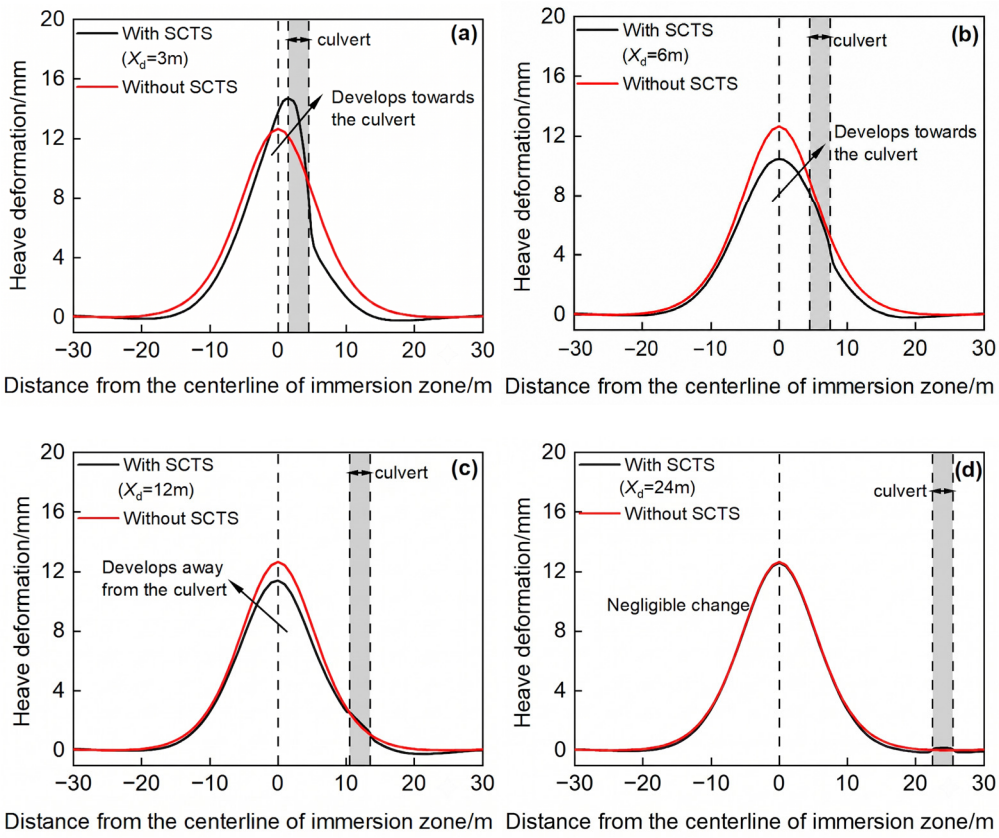

Figure 18. Comparison of railway subgrade heave deformation for different water immersion zone locations: (**a**) X_d = 3 m; (**b**) X_d = 6 m; (**c**) X_d = 12 m; (**d**) X_d = 24 m.

4.5. Gray Relational Analysis of Influencing Factors on Subgrade Heave Deformation

4.5.1. Gray Relational Analysis Method

To quantitatively compare the relative influences of immersion zone width, swelling potential, and immersion location on the maximum heave and width of heave area, Gray Relational Analysis (GRA) was adopted. GRA is suitable for engineering problems involving small sample sizes, multiple influencing factors, and partially incomplete information [44]. It evaluates the degree of association by comparing the geometric similarity between the sequences of influencing factors and the response indicator sequence. The calculation procedure for determining the gray relational grades between the influencing factors and response indicators is given in Equations (6)–(9):

1. Dimensionless normalization. To eliminate the influence of different dimensions and magnitude levels among variables, the original data were normalized using the min–max method. For a positive indicator, the normalized sequence is expressed as

$$X_i(k) = (x_i(k) - \min(x_i))/(\max(x_i) - \min(x_i)) \quad (6)$$

where $x_i(k)$ is the original value of the i-th sequence at the k-th data point; $X_i(k)$ is the corresponding normalized value.

2. Calculation of absolute differences. The absolute difference between the normalized reference sequence $X_0(k)$ and each comparative sequence $X_i(k)$ was calculated as

$$\Delta i(k) = (X_0(k) - X_i(k)) \quad (7)$$

3. Calculation of gray relational coefficients. The gray relational coefficient was calculated to measure the local similarity between the reference sequence and each comparative sequence at each data point:

$$\xi_i(k) = (\Delta_{\min} + \rho\Delta\max)/(\Delta i(k) + \rho\Delta\max) \quad (8)$$

where $\xi i(k)$ is the gray relational coefficient, and ρ is the distinguishing coefficient, which is taken as 0.5.

4. Calculation of gray relational grades. The gray relational grade was obtained by averaging the gray relational coefficients over all data points:

$$\gamma_i = \frac{1}{n}\sum \xi_i(k) \quad (9)$$

where γ_i is the gray relational grade of the i-th comparative sequence relative to the reference sequence.

4.5.2. Analysis of Ranking Results

When the immersion location X_d ranges from 0 to 3 m, the immersion zone covers the expansive soil foundation beneath or near the transition structure. However, in engineering practice, the immersion zone should be kept away from the SCTS. Therefore, in the gray relational analysis, the immersion location calculated starting from X_d was 6 m to avoid possible nonlinear effects.

As shown in Table 3, both the immersion zone width and the swelling potential show relatively high gray relational grades with the maximum heave deformation, with values of 0.89 and 0.87, respectively. The small difference between these two values indicates that both the immersion range and the swelling potential of the foundation have important effects on heave deformation.

Table 3. Gray relational degrees between heave deformation characteristics and influencing factors.

Influencing Factor	γ (Heave Deformation)	γ (Width of Heave Area)
Width of the water immersion zone (L)	0.89	0.93
Swelling potential α	0.87	0.74
Location of the water immersion zone X_d	0.65	0.61

For the width of heave area, the gray relational grade of the immersion zone width is 0.93, which is higher than that of the swelling potential, 0.74. This indicates that the expansion of the immersion zone can enlarge the width of heave area of the expansive soil foundation, while the influence of swelling potential is relatively secondary. The local gray relational grades between immersion location and maximum heave deformation and between immersion location and width of heave area are 0.65 and 0.61, respectively, which are lower than those of immersion zone width and swelling potential. When the immersion zone gradually moves away from the culvert, the influence of immersion location on heave deformation decreases.

Therefore, in the prevention and control of heave deformation in railway SCTS on expansive soil foundations, priority should be given to strengthening drainage and anti-seepage measures in the SCTS. Multiple intercepting drains may be arranged outside the culvert structure to reduce local water accumulation and infiltration near the SCTS. For sections with relatively high swelling potential, soil replacement or soil improvement measures can be adopted to reduce the influence of swelling–shrinkage deformation of the foundation. Particular attention should be paid to differential heave deformation caused by

changes in local immersion location near the culvert, so as to reduce the risk of structural unevenness and track irregularity in the SCTS.

5. Conclusions

Based on the in situ vertical swelling pressure test (measured at 61.5 kPa) and the temperature–humidity equivalent theory, the equivalent thermal expansion coefficient (α) was back-calculated to be 7.228×10^{-4} °C^{-1} via the equivalence of temperature-induced expansion and swelling reaction force. Subsequently, a 3D numerical model of the SCTS on an expansive soil foundation was established to investigate the effects of water immersion zone width, location, and swelling potential on the subgrade heave characteristics. The main conclusions are as follows:

1. When the immersion width increased from 2 m to 10 m, the subgrade heave deformation increased from 8.746 mm to 22.495 mm, and the width of heave area expanded from 22.648 m to 32.656 m. When the swelling potential parameter α increased from 5.0×10^{-4} °C^{-1} to 9.0×10^{-4} °C^{-1}, the subgrade heave deformation increased from 11.585 mm to 21.288 mm, whereas the width of heave area only increased from 27.524 m to 28.450 m.
2. As the distance between the centerline of the foundation immersion zone and the culvert center increased, the subgrade heave deformation showed a trend of first decreasing and then increasing. When the immersion zone covered the area beneath the culvert, the subgrade heave deformation reached its maximum and caused overall uplift of the culvert. When the immersion zone was unevenly distributed beneath the culvert, differential heave deformation of the SCTS could be induced. Therefore, in engineering practice, water immersion should be prevented from occurring near the culvert as much as possible.
3. Gray relational analysis indicated that both immersion width and swelling potential were closely associated with the maximum heave deformation, while immersion width was closely associated with the width of heave area. The correlations between immersion location and both heave deformation and width of heave area were relatively lower, mainly because the influence of foundation heave deformation decreases as the immersion zone moves away from the culvert. In engineering practice, priority should be given to controlling the immersion range of the foundation near the SCTS, improving interception–drainage and anti-seepage measures, and adopting soil improvement measures for expansive soil foundations.
4. The present study focuses on the heave deformation characteristics of expansive soil foundations in the SCTS under adverse immersion conditions, with emphasis on the surface deformation response under water immersion. Future research should further investigate the mechanical response of the SCTS and validate the numerical results using field monitoring data obtained under long-term service conditions.

Author Contributions: Conceptualization, Q.L. and J.Y.; methodology, Y.Z. and Z.Z.; software, Q.L. and Z.D.; validation, Y.Z., Z.Z. and Z.D.; formal analysis, T.W. and Y.L.; investigation, Q.L.; resources, H.Z. and S.L.; data curation, Q.L. and T.W.; writing—original draft preparation, Q.L.; writing—review and editing, Z.Z., Z.D. and J.Y.; visualization, Q.L. and S.L.; supervision, Y.Z., H.Z. and Y.L.; project administration, J.Y.; funding acquisition, Y.Z. and H.Z. All authors have read and agreed to the published version of the manuscript.

Funding: This study was supported by the Guangxi Key Research and Development Program (Grant No. AB23075184), the National Natural Science Foundation of China (Grant No. 42477143), the Guangxi Major Talent Program, the Key Program of the National Natural Science Foundation of

China (Grant No. 42330701), and the Guangxi Transportation Science and Technology Achievement Promotion Project (Grant No. GXJT-ZDSYS-2023-03-01).

Data Availability Statement: The raw data supporting the conclusions of this article will be made available by the authors on request.

Conflicts of Interest: Authors Tao Wu, Yangpeng Zhang, Hongri Zhang, Shiyi Luo and Jiming Yang were employed by the Guangxi Transportation Science and Technology Group Co., Ltd. Author Zhen Zhang was employed by Railway Engineering Research Institute, China Academy of Railway Sciences Co., Ltd. The remaining authors declare that the research was conducted in the absence of any commercial or financial relationships that could be construed as a potential conflict of interest.

References

1. Agarwal, B.K.; Sachan, A. X-ray CT-based 3D characterization of desiccation cracking in compacted expansive soil under varying vertical stress states. *Acta Geotech.* **2025**, *20*, 5221–5242. [CrossRef]
2. Luo, Y.; Zhang, J.; Tang, C.-S.; Jiang, G.; Bogaard, T. Impact of dynamic desiccation cracks on hydrological processes and stability in expansive clay slopes: A coupled dual-permeability modeling approach. *Eng. Geol.* **2025**, *357*, 108377. [CrossRef]
3. Zheng, J.; Zhang, R.; Yang, H. Highway subgrade construction in expansive soil areas. *J. Mater. Civ. Eng.* **2009**, *21*, 154–162. [CrossRef]
4. Arif, R.; Feng, T.; Zhang, K.; Su, Z. Field and numerical investigation of Taihu Resort cut slope failure in Suzhou, China. *Appl. Sci.* **2024**, *14*, 2683. [CrossRef]
5. Mohammed, F.; Jibril, J.; Sorsa, A.; Alemu, C.; Chakeri, D. Experimental study on expansive subgrade clay soils stabilized with sugarcane bagasse ash and nonwoven geotextile. *Adv. Civ. Eng.* **2024**, *2024*, 8259830. [CrossRef]
6. Tanyıldızı, M.; Uz, V.; Gökalp, İ. Utilization of waste materials in the stabilization of expansive pavement subgrade: An extensive review. *Constr. Build. Mater.* **2023**, *398*, 132435. [CrossRef]
7. Dai, Z.J.; Guo, J.; Yu, F.; Zhou, Z.; Li, J.; Chen, S. Long-term uplift of high-speed railway subgrade caused by swelling effect of red-bed mudstone: Case study in Southwest China. *Bull. Eng. Geol. Environ.* **2021**, *80*, 4855–4869. [CrossRef]
8. Krishna, P.; Murty, V. Long-term field heave studies on various foundation techniques in expansive soils. *Indian Geotech. J.* **2021**, *51*, 909–923. [CrossRef]
9. Tang, A.; Cui, Y.; Trinh, V.; Szerman, Y.; Marchadier, G. Analysis of the railway heave induced by soil swelling at a site in southern France. *Eng. Geol.* **2009**, *106*, 68–77. [CrossRef]
10. Zeng, Z.; Ye, M.; Wang, W.; Liu, J.; Shen, S.; Qahtan, A. Analysis on mechanical characteristics of CRTSII slab ballastless track structures in rectification considering material brittleness. *Constr. Build. Mater.* **2022**, *319*, 126058. [CrossRef]
11. Zhang, W.; Hu, Q.; He, L.; Gu, Y.; Zeng, J.; He, L. Experimental investigation on the applicability of microwave-modified red-bed soft rock subgrade filler. *J. Mater. Civ. Eng.* **2023**, *35*, 04023451. [CrossRef]
12. Yan, H.; Zhao, X.; Wünnemann, B.; Jian, L.; Chen, M.; Xiao, D. A method for predicting the subgrade uplift intensity along a high-speed railway track in red-bed areas in China. *Bull. Eng. Geol. Environ.* **2023**, *82*, 303. [CrossRef]
13. Xue, Y.; Wang, Q.; Ma, L.; Yu, Y.; Zhang, R. Calculation model of heaving amount on embankments using multi-factor coupling of low swell potential mudstone as foundation for high-speed railways. *Transp. Geotech.* **2023**, *38*, 100924. [CrossRef]
14. Feng, Y. Study on Load Transfer Law and Deformation Characteristics of Expansive Soil Beneath High-Speed Railway Subgrades. Ph.D. Thesis, Southwest Jiaotong University, Chengdu, China, 2018.
15. Jiang, G.; Chen, W.; Liu, X.; Yuan, S.; Wu, L.; Zhang, C. Field study on swelling-shrinkage response of an expansive soil foundation under high-speed railway embankment loads. *Soils Found.* **2018**, *58*, 1538–1552. [CrossRef]
16. Cao, Z. Field soaking tests on high-speed railway subgrades in medium-strong expansive soil areas. *J. Railw. Sci. Eng.* **2022**, *19*, 3467–3476.
17. Duan, J.; Liang, S.; Su, Y.; Lin, Y.; Liu, W.; Wang, G.; Lu, L. Experimental investigation of the heave behaviors of ballastless railways on expansive soil foundations. *Transp. Geotech.* **2025**, *52*, 101544. [CrossRef]
18. Duan, J.; Yang, G.; Hu, M.; Lei, X.; Lin, Y. Swelling characteristics of andesite foundation induced by water immersion and their influence on ballastless track subgrade. *J. Mt. Sci.* **2020**, *17*, 1001–1012. [CrossRef]
19. Duan, J.; Yang, G.; Hu, M.; Wang, G.; Lin, Y. Heave performance of a ballastless track subgrade of double-line high-speed railway filled with micro-expansive andesite under water immersion. *Constr. Build. Mater.* **2020**, *252*, 119087. [CrossRef]
20. Yu, Y.; Ding, X.; Ma, L.; Cui, W.; Du, Q. Experimental study on in-situ water infiltration response characteristics of micro-expansive mudstone foundation. *Rock Soil Mech.* **2024**, *45*, 647–658. [CrossRef]
21. Xue, Y.; Wang, Q.; Ma, L.; Yu, Y.; Zhang, R. Mechanisms and controlling factors of heave in summer for high-speed railway cutting: A case study of Northwest China. *Constr. Build. Mater.* **2023**, *365*, 130061. [CrossRef]

22. Wang, R.; Cheng, J.; Gao, L.; Li, Z.; Qi, Y.; Wang, M.; Ding, B.S. Research on the swelling mechanism of high-speed railway subgrade and the induced railway heave of ballastless tracks. *Transp. Geotech.* **2021**, *27*, 100470. [CrossRef]
23. Wang, R.; Yan, B.; Ding, B.; Wang, Y.; Cheng, J. Evaluating the impact of mudstone swelling on railway heave of ballastless tracks in the transition section using the DEM-FDM coupling method. *Int. J. Geomech.* **2024**, *24*, 04024264. [CrossRef]
24. Yang, J.; Zhang, H.; Ni, P. DEM analysis of stress state, fabric anisotropies and failure behavior in multi-layer stacked soilbags under geotextile-soil interlocking reinforcement. *Constr. Build. Mater.* **2024**, *452*, 138958. [CrossRef]
25. Wang, Z.; Zhang, L.; Cheng, H.; Zhang, X. Numerical simulation analysis of failure mechanism of expansive soil canal based on thermo-hydro-mechanics three-field coupling. *Arch. Appl. Mech.* **2025**, *95*, 186. [CrossRef]
26. Yan, Y.; Zhang, Y.; Shen, Q.; Wang, C. Numerical analysis of internal force distribution in combining supporting structures for expansive soil high slope along railway. *Buildings* **2024**, *14*, 3081. [CrossRef]
27. Duan, J.; Cao, P.; Su, Y.; Lin, Y.; Yang, G. Influence of swelling characteristics of expansive soil foundations on the deformation performance of ballastless-track subgrades. *J. Cent. South Univ. Sci. Technol.* **2024**, *55*, 3530–3542.
28. Zhao, W.; Zhang, K.; Han, F.; Wang, D. Study on the reducing measures to reduce the influence of culvert extension on existing lines in loess regions. *Appl. Sci.* **2023**, *13*, 4138. [CrossRef]
29. Varandas, J.; Hölscher, P.; Silva, M. Three-dimensional track-ballast interaction model for the study of a culvert transition. *Soil Dyn. Earthq. Eng.* **2016**, *89*, 116–127. [CrossRef]
30. Esmaeili, M.; Heydari-Noghabi, H.; Kamali, M. Numerical investigation of railway transition zones stiffened with auxiliary rails. *Proc. Inst. Civ. Eng. Transp.* **2018**, *173*, 299–308.
31. Hassan, A.; Khalil, A.; El-Sonbaty, A.; Ahmed, H. Comparative numerical study on the performance of different mitigation techniques in high-speed railway transition zones. *Soil Dyn. Earthq. Eng.* **2026**, *206*, 110256. [CrossRef]
32. Bagchi, A.; Raychowdhury, P. Railway bridge end-approach zone under a moving load: Numerical assessment from a geotechnical perspective. *Int. J. Geomech.* **2025**, *25*, 04025004. [CrossRef]
33. *TB 10025-2019*; Code for Design of Retaining Structures of Railway Earthworks. China Railway Publishing House: Beijing, China, 2019.
34. Lü, X.L.; Zhong, Y.S.; Xue, D.W.; Su, Z.; Du, H.H. Numerical analyses for the bearing behavior and uplift potential of single pile in water-sensitive expansive soils. *Geomech. Eng.* **2025**, *41*, 365–380.
35. *TB 10621-2014*; Code for Design of High Speed Railway. China Railway Publishing House: Beijing, China, 2014.
36. Zhao, J.; Tan, Z.; Wang, X.; Zhou, Z.; Li, G. Engineering characteristics of water-bearing weakly cemented sandstone and dewatering technology in tunnel excavation. *Tunn. Undergr. Space Technol.* **2022**, *121*, 104316. [CrossRef]
37. Zhao, J.; Tan, Z.; Li, L.; Yu, R.; Lei, K. Visco-elastic-plastic creep model based on Burgers and Bingham model and its verification. *Arab. J. Geosci.* **2022**, *15*, 479. [CrossRef]
38. Zhao, J.; Tan, Z.; Li, L.; Wang, X. Supporting structure failure caused by the squeezing tunnel creep and its reinforcement measure. *J. Mt. Sci.* **2023**, *20*, 1774–1789. [CrossRef]
39. Deng, Z. Study on Characteristics of Expansive Soil Ground Uplift Deformation and Its Influence on Railway Subgrade. Master's Thesis, Central South University, Changsha, China, 2023.
40. Cai, Y.; Xu, L.; Liu, W.; Shang, Y.; Su, N.; Feng, D. Field test study on the dynamic response of the cement-improved expansive soil subgrade of a heavy-haul railway. *Soil Dyn. Earthq. Eng.* **2020**, *128*, 105878. [CrossRef]
41. *TB 10102-2010*; Code for Soil Test of Railway Engineering. China Railway Publishing House: Beijing, China, 2010.
42. *GB 50112-2013*; Technical Code for Buildings in Expansive Soil Areas. China Architecture and Building Press: Beijing, China, 2012.
43. Soltani, A.; Taheri, A.; Khatibi, M.; Estabragh, A.R. Swelling Potential of a Stabilized Expansive Soil: A Comparative Experimental Study. *Geotech. Geol. Eng.* **2017**, *35*, 1717–1744. [CrossRef]
44. Zhang, C.; Zhang, Q.; Jiang, J.; Yang, Q. Pullout properties of *Hippophae rhamnoides* L. roots in the loess area. *Arch. Agron. Soil Sci.* **2023**, *69*, 2170–2186.

Disclaimer/Publisher's Note: The statements, opinions and data contained in all publications are solely those of the individual author(s) and contributor(s) and not of MDPI and/or the editor(s). MDPI and/or the editor(s) disclaim responsibility for any injury to people or property resulting from any ideas, methods, instructions or products referred to in the content.